

PCCP

Accepted Manuscript



This is an *Accepted Manuscript*, which has been through the Royal Society of Chemistry peer review process and has been accepted for publication.

Accepted Manuscripts are published online shortly after acceptance, before technical editing, formatting and proof reading. Using this free service, authors can make their results available to the community, in citable form, before we publish the edited article. We will replace this *Accepted Manuscript* with the edited and formatted *Advance Article* as soon as it is available.

You can find more information about *Accepted Manuscripts* in the [Information for Authors](#).

Please note that technical editing may introduce minor changes to the text and/or graphics, which may alter content. The journal's standard [Terms & Conditions](#) and the [Ethical guidelines](#) still apply. In no event shall the Royal Society of Chemistry be held responsible for any errors or omissions in this *Accepted Manuscript* or any consequences arising from the use of any information it contains.

A multinuclear solid state NMR spectroscopic study of the structural evolution of disordered calcium silicate sol-gel biomaterials

Zhongjie Lin^a, Julian R. Jones^b, John V. Hanna^{a,*} and Mark E. Smith^{a,c,*}

- a. Magnetic Resonance Centre, Millburn House, Department of Physics, University of Warwick, Coventry, CV4 7HS, UK
- b. Department of Materials, Imperial College London, London, SW7 2BP, UK
- c. Vice-Chancellor's Office, University House, Lancaster University, LA1 4YW, UK

Abstract

Disordered sol-gel prepared calcium silicate biomaterials show significant, composition dependent ability to bond with bone. Bone bonding is attributed to rapid hydroxycarbonate apatite (HCA) formation on the glass surface after immersion in body fluid (or implantation). Atomic scale details of the development of the structure of $(\text{CaO})_x(\text{SiO}_2)_{1-x}$ ($x = 0.2, 0.3$ and 0.5) under heat treatment and subsequent dissolution in simulated body fluid (SBF) are revealed through a multinuclear solid state NMR approach using one-dimensional ^{17}O , ^{29}Si , ^{31}P , ^{43}Ca and ^1H . Central to this study is the combination of conventional static and magic angle spinning (MAS) and two-dimensional (2D) triple quantum (3Q) ^{17}O NMR experiments that can readily distinguish and quantify the bridging (BOs) and non-bridging (NBOs) oxygens in the silicate network. Although soluble calcium is present in the sol, the ^{17}O NMR results reveal that the sol-gel produced network structure is initially dominated by BOs after gelation, aging and drying (e.g. at 120°C), indicating a nanoscale mixture of the calcium salt and a predominantly silicate network. Only once the calcium salt is decomposed at elevated temperatures do the Ca^{2+} ions become available to break BO. Apatite forming ability in SBF depends strongly on the surface OH *and* calcium content. The presence of calcium aids HCA formation via promotion of surface hydration and the ready availability of Ca^{2+} ions. ^{17}O NMR shows the rapid loss of NBOs charge balanced by calcium as it is leached into the SBF. The formation of nanocrystalline, partially ordered HCA can be detected via ^{31}P NMR. This data indicates the importance of achieving the right balance of BO/NBO for optimal biochemical response and network properties.

* Authors for correspondence:

J. V. Hanna: Department of Physics, University of Warwick, Coventry, UK, CV4 7AL

Email: J.V.Hanna@warwick.ac.uk

M. E. Smith: Vice-Chancellor's Office, University House, Lancaster University, LA1 4YW, UK and Department of Physics, University of Warwick, Coventry, UK, CV4 7AL.

Email: M.E.Smith@lancaster.ac.uk

1. Introduction

Increasing human longevity in many countries has resulted in ever more people outliving the quality of their musculoskeletal tissues. This has consequently demanded development of biomaterials for bone regeneration. Various sol-gel prepared bioactive gel-glass materials have been developed in the last few decades, with some of them finding successful commercial applications.¹⁻⁸ Most bioactive glasses have evolved from a somewhat trial-and-error approach historically, so that it is unsurprising that the optimal bioactive features have not been rapidly achieved. Further improvement of these materials therefore demands a fundamental understanding of their behaviour. For sol-gel glasses, the glass structure evolves through a bottom up assembly of silica nanoparticles and the atomic level structure evolves during heat treatment. It also changes with subsequent reaction with blood or simulated body fluid (SBF).

Bioactive glasses can act as a bone tissue engineering scaffold⁹ for cell adherence^{10,11}, growth and bone regeneration have been developed and some of the most successful series are sol-gel prepared calcium silicate based biomaterials.³⁻¹⁶ These sol-gel prepared bioactive glasses offer a number of potential advantages over traditional melt-quench materials such as lower processing temperature, straightforward composition variation, higher purity and homogeneity, textural porosity and larger surface area. It has been discovered that calcium silicate based bioactive glasses activate several families of genes in human bone cells with associated release of soluble silicate and calcium ions in very specific concentrations.^{17,18} The bonding of bioactive glasses with living tissue is related to the formation of a layer consisting of carbonate-containing hydroxyapatite [HCA] on the surface of the materials.¹⁹ *In vivo* studies of the surface reactions of sol-gel CaO-SiO₂ glasses show that they rapidly regenerate bone defects if the composition and pore size are appropriate.²⁰

In studying complex, disordered solid materials, combinations of leading-edge characterisation techniques are important to give real insight into the main underlying structural features. Solid state NMR is one of the key techniques as an element specific probe with good sensitivity to the local structural environment in a wide range of inorganic materials.^{21,22} In bioactive sol-gel prepared calcium silicates ²⁹Si and ¹H have been the most studied nuclei.⁷ Although high resolution ¹⁷O solid-state NMR has been successfully applied in the structural study of several kinds of silicate materials²¹⁻²⁸ and mixed oxides²⁹⁻³¹ it has yet to be extensively applied to such disordered sol-gel prepared calcium silicates. In sol-gel prepared silicate mixed oxides (i.e. silica with another oxide added) ¹⁷O NMR has been shown to be a very direct way of probing network ordering and condensation.³²⁻³⁴ The large

chemical shift range of ^{17}O with its ability to distinguish bridging (BOs), non-bridging oxygens (NBOs) and the other structural fragments that the oxygen is involved in (e.g. metal-O-metal, OH, etc.) is much more direct evidence on the details of the structure than from ^{29}Si NMR. The direct observation of different oxygen species then ties down more definitively the silicate network connectivity, atomic scale mixing and phase separation in such materials.

Research by the group to date has used a combination of diffraction, X-ray absorption spectroscopy and ^{29}Si solid state NMR to understand the role of calcium in such sol-gel prepared calcium silicate based bioactive sol-gel materials, especially when calcium nitrate is used as a precursor. However there is still no detailed report of solid state NMR for such sol-gel formed calcium silicate bioactive glasses which combines ^{29}Si with ^{17}O to follow directly the formation NBOs created during heat treatment when the calcium nitrate decomposes. There has also been no NMR studies of the effects of the subsequent loss of calcium from the network during reaction with SBF. A comprehensive multinuclear NMR investigation of sol-gel formed $(\text{CaO})_x(\text{SiO}_2)_{1-x}$ materials specifically related to bioactive compositions of scientific and technological significance with $x = 0.2, 0.3$ and 0.5 (denoted 80S20C, 70S30C and 50S50C) using ^{17}O , ^{29}Si , ^{31}P and ^1H solid state NMR is presented here. The key aim here is to establish in detail the change of NBOs associated with calcium during formation and subsequent reaction and hence better understand the relationship between composition-structure-biochemical properties of such sol-gel produced CaO-SiO₂ materials.

2. Experimental

2.1 Sol-Gel Sample Preparation, Heat Treatment and SBF Reaction

The ^{17}O -enriched $(\text{CaO})_x(\text{SiO}_2)_{1-x}$ samples studied here were synthesised using a sol-gel route from the following materials: tetraethyl orthosilicate, TEOS (Aldrich, 98%), $\text{Ca}(\text{NO}_3)_2 \cdot 4\text{H}_2\text{O}$ (Aldrich, 99%), 1M HNO_3 (Aldrich), anhydrous ethanol (Aldrich, 99.9%). For the one-dimensional (1D) ^{17}O MAS NMR measurements 10 mol% ^{17}O -enriched water (D-Chem) was used, however for the 2D 3QMAS measurements a higher ^{17}O enrichment was sought by using 40 mol% water (Cortecnet). Preparation was by two-stage hydrolysis with TEOS hydrolysed first. In these reactions the molar ratio of the different components, TEOS:ethanol:H₂O, was 1:2:2. At these ratios in principle all of the ^{17}O label should end up initially in the sample, although some losses are inevitable and these losses increase with heat treatment.³⁵ Following this initial mixing calcium nitrate was added. Gels were prepared at three different $(\text{CaO})_x(\text{SiO}_2)_{1-x}$ compositions ($x = 0.2, 0.3$ and 0.5). The hydrolysis reaction was usually continued for 8-15 hours under acidic catalysis and stirring.

Then the clear sol was transferred to small polythene bottles and sealed to gel, followed by ageing at room temperature. The screw tops were loosened for drying at 70-80 °C for 3-5 days. The resulting dry gel was then heated at 2-5 °C/min. to the desired temperature (120, 350, 500 and 700 °C) for 1-2 hours under an N₂ or Ar atmosphere to minimise the loss of ¹⁷O.³⁵ The SBF solution was prepared according to an accepted procedure so that it contained a similar concentration of ions to blood plasma³⁶, although there is some debate as to whether or not SBF is a good *in vitro* test.³⁷ The SBF reaction of the samples was carried out using 0.1-0.2 g of powder sample with 3-4 ml of SBF solution in a small glass vessel and placed in a water bath with the temperature kept at 37±0.1 °C. The sample after reaction was filtered and washed intensively with acetone and dried in an oven at 70 °C for 8 hours.

2.2 NMR Measurements

All 1D ¹⁷O MAS NMR data were acquired at 14.1 T (data used in the figures) and 8.45 T using Bruker AvanceII+-600 and Varian Chemagnetics CMX 360 spectrometers operating at ¹⁷O Larmor frequencies of 81.3 and 48.8 MHz, respectively. These ¹⁷O MAS NMR data were measured with a rotor-synchronised echo (θ - τ -2 θ) experiment,³⁸ using a Bruker 4 mm HX probe in which MAS frequencies of 12 kHz were achieved. The τ delay of the echo sequence was set to the inverse of the MAS frequency, with a recycle delay of 1 s duration being sufficient to prevent saturation. ¹⁷O MAS NMR data with a good signal-to-noise can be acquired in experiment times ranging from 10 minutes to about 12 hours depending the actual level of ¹⁷O enrichment achieved with each sample. The 2D ¹⁷O 3QMAS NMR data was acquired at 14.1 and 11.7 T using Bruker AvanceII+-600 and Bruker AvanceIII-500 spectrometers, the latter operating at a ¹⁷O Larmor frequency of 67.8 MHz. These measurements were also undertaken using a Bruker 4 mm HX probe which enabled samples spinning at 15 kHz. These data were measured using a three pulse z-filter experiment^{39,40} which acquired 384 transients per F2 increment (basic phase cycle 96) with a recycle delay of 1-1.5 s and more than 100 F1 increments. Typical pulses widths for the excitation, conversion and soft z-filter pulses were 4.5, 1.5 and 30 μ s, respectively. The ¹⁷O NMR spectra were referenced externally to H₂O at 0 ppm. Shearing and referencing was done within the Bruker software using one of the standard conventions.⁴¹

Corresponding ³¹P and ²⁹Si MAS NMR data were acquired at 8.45 T using a Varian Chemagnetics CMX-360 spectrometer operating at ³¹P and ²⁹Si Larmor frequencies of 145.8 and 71.5 MHz, respectively. The ³¹P measurements used a Bruker 4 mm HX probe which enabled sample spinning at 6-8 kHz, with no ¹H decoupling. These data were acquired with a

single pulse experiment and a recycle delay of 1 s, with referencing to the primary standard of 85% H_3PO_4 was performed via a secondary solid reference $(\text{NH}_4)\text{H}_2\text{PO}_4$ at 0.9 ppm. The ^{29}Si MAS NMR data were acquired using a Bruker 7 mm probe which enabled sample spinning at 5 kHz. Single pulse experiments typically used a tip angle of 30° and recycle delays of 30-40 s, with spectra were referenced externally to TMS at 0 ppm. Each spectrum was the result of summing 1000-2000 transients. Quantitative ^1H MAS NMR measurements were undertaken at 8.45 T using a Varian Chemagnetics CMX-360 spectrometer operating at a ^1H Larmor frequency of 360.12 MHz. A Bruker 4 mm HX probe was used which allowed MAS frequencies of 12 kHz and provided sufficient narrowing for clear integration of the spectral intensity associated with the sample. Single pulse experiments with a recycle delay of 20 s were employed, where the integrated intensity of each ^1H spectra was used to estimate the proton content of the gel-prepared samples. Quantification of the proton content was achieved by calibration against a reference adamantane sample as a standard for quantification using identical experimental conditions and spectral processing and scaling for the sample mass and number of scans used. The ^1H NMR data were referenced externally to TMS at 0 ppm.

3. Results and Discussion

3.1 Structural Development of Gel-Produced Calcium Silicates with Heat Treatment

The ^{17}O NMR results reveal that at low heat treatment temperature (120°C), the network structure is dominated by the second-order quadrupolar lineshape^{21,42} of the BOs (Si-O-Si), but with contributions from Si-OH at around 0 ppm as can be seen by the more positive singularity of the quadrupolar powder pattern having higher intensity than expected for such a powder pattern from a single second-order quadrupolar broadened site (Fig. 1).^{21,23,42} The static ^{17}O NMR spectra (Fig. 2) from 80S20C more clearly shows the hydroxyls presence in the sample heated to just 120°C as there is a much sharper resonance from the hydroxyl centred at 0 ppm, on top of the very much broader second-order quadrupolar lineshape of the BO. The hydroxyl peak disappeared from the static spectrum after the sample was heated at 350°C indicating the reduction in intensity of this species. The ^{17}O NMR data presented here now directly corroborates previous ^{29}Si MAS NMR data (and repeated here below) that indicates via the inference from the connectivity of the silicate network that the Ca^{2+} ions are not yet intimately part of that network at 350°C as there is no strong NBO peak, with the calcium probably remaining as a layer of the initial calcium salt on the primary silica particles.⁷

Hence after moderate heat treatment up to 350 °C, the silicate network appears to have become more condensed through the loss of OH groups, although some very weak NBO ^{17}O signal begins to appear at around 70-90 ppm (Fig. 3b), perhaps from some very modest calcium exchange. The dominant change in the silicate network is the hydroxyl loss and the relative lack resolution of the ^{29}Si MAS NMR spectra from a disordered silicate means that small changes associated with any low NBO presence may not yet be visible. At higher temperatures (≥ 500 °C), the NBOs become much more significant, indicating that calcium now plays a much more central role in the silicate network and begins to dominate changes in it (Fig. 4). The calcium species migrate into the silicate network, acting as a network modifier and gradually break the Si-O-Si BOs, forming NBOs. There are two variables that allow the unequivocal identification of the NBO signal, the change of the relative intensity with both increasing heat treatment and calcium content. The intensity of the NBO resonance at around 70-90 ppm (peak position) increases with increasing CaO content from 20 to 50 mol% (Fig. 4) in these materials, as well as with increasing treatment temperature (Fig. 5). For the integrated data any associated sideband intensity was included. This 70-90 ppm resonance is assigned to NBO associated with calcium because the intensity of this resonance shows direct correlation with CaO content. It also has a smaller linewidth and hence smaller quadrupole interaction (χ_Q) compared to that for the BO due to the more ionic nature of the bonding of an NBO.²³ The field variation of the spectra (e.g. the changes in widths and overall peak/centre of gravity position) along with where there were clear second-order quadrupolar features allowed the quadrupolar interaction to be estimated. A smaller χ_Q of 3-3.3 MHz was thereby determined for NBO (Table 1) compared to χ_Q of 4.2-4.9 MHz for BO, in good agreement with known data in crystal and other amorphous silicate materials.^{21,23} It should be noted that in many metal silicate systems the actual linewidths, along with the relative isotropic chemical shifts and second-order quadrupole shifts mean that there is often strong overlap between the BO and NBO ^{17}O signals, but the combination of parameters for the calcium silicate system means that unusually there is excellent resolution even in one dimensional ^{17}O MAS NMR spectra.

The 2D ^{17}O 3QMAS data acquired at 11.7 and 14.1 T for S70C30 samples heat treated at 350 and 600 °C are shown in Figure 6. These data were used to confirm that no underlying species were present which may be obscured by the broad BO resonance. The sheared data clearly shows the dominance of the BO at 350 °C (see Figures 6(a) and 6(c)) and the appearance of the NBO at 600 °C (see Figures 6(d) and 6(d)), with no other enriched oxygen species (especially those attributable to OH species) being detected in these preparations. These data also demonstrate that for the BO species the second-order

quadrupolar effects dominate as the 2D ^{17}O quadrupolar lineshape is parallel to the horizontal (F2 or MAS) axis, whereas for the NBO chemical shift dispersion more strongly influences this resonance as the contours exhibit a trajectory which closely aligns with the chemical shift (CS) axis for a spin $5/2$ nucleus. The disordered nature of these samples is further emphasised by comparing the 3QMAS data acquired at 11.7 T with that similarly acquired at 14.1 T. This increase in B_0 field produces broader resonances in the isotropic (F1) projection due to the linear field dependence of the chemical shift dispersion distribution with B_0 (compare Figures 6(a) and 6(b) with 6(c) and 6(d)). It should be noted that there is the need for care in interpreting such linewidths as changes in scaling during the processing or differential MQ excitation in different cases.^{21,43} Although here the observed changes with field are believed to support the suggested change in chemical shift dispersion. Also it should be noted that such an MQ spectrum would probably largely miss any enriched –OH present due to the much smaller χ_Q leading to inefficient MQ excitation and more strongly relaxing nature of such oxygens reducing any echo strength.⁴⁴

An increase in the NBO resonance intensity in the ^{17}O MAS NMR spectra is as a result of a modification of the silicate network and should cause a concomitant increase in the intensities of the ^{29}Si Q^2 and Q^3 resonances. Such an anticipated change in the ^{29}Si intensities agrees with previous ^{29}Si MAS NMR data⁷ and is confirmed by the ^{29}Si NMR data presented here (see Table 2). The ^{29}Si NMR data clearly show that increasing intensities of the Q^2 and Q^3 resonances are associated with an increasing intensity of the NBO resonance observed in the ^{17}O NMR. The identification of this NBO resonance is straightforward and its intensity is directly related to the CaO content of the materials. For example, the Q^2 content increases from 3.3 to 50.4 % as the CaO content increased from 20 % to 50 % and heat treated at 500 °C. Correspondingly the NBO signal intensity increases from 7 % to 50.1 % for same set of samples (Table 1).

After heat treatment at temperatures > 500 °C, the chemical shifts of both BO and NBO resonances display a positive shift with increasing Ca/Si ratio in the materials, which reflect the changes in oxygen shielding and decrease in the average polymerisation of the silicate network. The effect of raising the heat treatment temperature on the chemical shift is the same as increasing Ca/Si ratio, since they both result in an increasingly large NBO resonance and decreasing polymerisation of the silicate network. The increasing chemical shifts can be understood as the consequences of deshielding effects when more Ca cations migrate into the silicate network forming larger amounts of NBO with more deshielded oxygen sites, subsequently also influencing the surrounding electron density of the BO resonances.

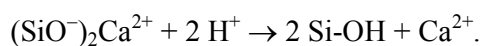
Some representative ^{29}Si MAS NMR spectra are shown in Figs 7 and 8, with the NMR parameters and relative intensities summarised in Table 2. After lower temperature heat treatment (120 °C) it can be seen (Table 2) that the Q^n species distribution of different compositions show no significant difference indicating a similar silicate network structure *despite* the differences in calcium content. This structural similarity is consistent with ^{17}O NMR results showing BO (Si-O-Si) dominating the network structure, as well as the presence of significant OH. This result is commonly found in sol-gel silicate materials that in the early stages of hydrolysis the silicate network is largely determined by the hydroxyl distribution and does not depend on the added metal as it is not participating in the silicate network at this point. At higher temperature (≥ 500 °C) calcium begins to disrupt the network as the nitrate breaks down and calcium needs to form NBO to satisfy its charge balancing requirements. Hence, the silicate network for this calcium silicate system is developed through two opposite trends which change in importance at higher heat treatment temperature. At lower temperatures there is removal of hydroxyls which increases network connectivity, while at higher temperatures ($\geq 500^\circ\text{C}$), there is decreasing network polymerisation caused by formation of NBO to charge balance the Ca^{2+} ions.

For samples with up to 30 mol% CaO, the chemical shifts of Q^4 , Q^3 and Q^2 species are around -110 , -100 and -90 ppm respectively, which is similar to aluminosilicate materials or some of mixed oxides. With 50 mol% CaO and heat treatment at 500 °C, Q^3 and Q^2 resonances are shifted to more positive positions at -96.5 and -78 ppm, presumably reflecting the increasing deshielding effects caused by much higher concentration of calcium in the network. On the assumption of having a continuous distribution of Q^n environments the resonance at -78 ppm is attributed to a calcium-rich Q^2 configuration, (i.e. $\text{Si}(\text{SiO})_2(\text{CaO})_2$), as opposed to say associated with some OHs, but there may be some overlap with Q^1 species. This assignment as a resonance associated with Q^2 seems reasonable considering that Q^2 resonance for alkali silicates (39% Li_2O) is at -80 ppm, and Q^2 for the identical composition crystal CaSiO_3 , β -wollastonite is at -83 ppm. β -wollastonite displays two sharp resonances at -111 and -83 ppm attributed to Q^4 and Q^2 silicon respectively.^{21,45} The difference in the ^{29}Si NMR data between 50S50C (500 °C) and β -wollastonite is the much broader resonances and existence of considerable amounts of Q^3 configuration (18.3 %) in 50S50C, reflecting the highly disordered state of the sample with large chemical shift dispersions and wide distributions of various bond lengths and bond angles.

We previously reported the ^{43}Ca MAS NMR data from exactly these samples as part of an extensive study of almost exclusively crystalline materials.⁴⁶ ^{43}Ca is a challenging nucleus although recent progress has been summarised in two recent reviews.^{47,48} The point relevant here is that the ^{43}Ca MAS NMR spectra with good S/N even at natural abundance could be collected from these gel samples heated to 120 and 350 °C. All these samples show a ^{43}Ca peak position still close to calcium nitrate^{46,47} which indicates that the calcium is distributed in a similar local environment and has not yet started to migrate into the silicate part of the structure, completely consistent with the above ^{17}O NMR results. At higher temperatures (500 °C) when large amounts of NBOs form, charge balanced by the Ca^{2+} ions, there is a very significant increase in the disorder round the calcium. This greatly increases the chemical shift distribution of the calcium sites ^{43}Ca such that it cannot then be readily observed.⁴⁶

3.2 Dissolution Mechanism and Hydroxyapatite Formation

^{17}O MAS NMR spectra of these sol-gel prepared samples after reacting with SBF show a rapid and significant decrease of the NBO intensity. The ^{17}O MAS NMR spectra of 80S20C after SBF reaction are shown in Fig. 9. After reaction for one hour, the sample shows significant reduction of NBO resonance which then effectively becomes absent after reaction for 24 hours. This is consistent with the ionic nature of NBO and indicates release of calcium ions can be very rapid, which produces large and rapid changes of the local concentration of calcium ions (this may be related to the mesoporosity of sol-gel materials and restricted diffusion in small pores and cages) as has been previously observed by X-ray fluorescence measurements of related systems.¹³ The presence of calcium and phosphate ions in solution (as well as carbonate from dissolved CO_2) near the surface promotes deposition and growth of a hydroxycarbonate apatite (HCA) layer. These silicon chains of the gel-formed calcium silicate framework are mainly held together by calcium-centred NBO bonds. With the rapid release of Ca^{2+} ions and decrease of such bonding some of the silicate framework can also be released into solution/body fluid as soluble silicate species. This process will lead to breaking of Si-O-Si bonds and formation of Si-OH at the surface.⁵ ^1H NMR can quantify the proton content (Table 3). The ^1H MAS NMR spectra (Fig. 10) show a resonance around 4 ppm with some showing another partially resolved peak at ~ 8 ppm. This work does not seek to fully identify the chemical nature of the protons present, which will be a mixture of Si-OH, and other proton species (e.g. some water is also present). The exchange of Ca^{2+} ions with H^+ could be a rapid process via an exchange such as



A further indication that the sites adjacent to the released Ca^{2+} sites are being reoccupied by H^+ to become a hydrated surface can be seen from ^{29}Si NMR result of 80S20C after one day of reaction with SBF. Although the ^{17}O MAS NMR data shows almost no NBOs associated with calcium remaining, the ^{29}Si NMR of this sample shows that the Q^2 (and Q^3) species are increased. Hence the release of Ca^{2+} not only increases the local concentration of calcium ions in the solution, but also promotes hydration of the surfaces, therefore providing favourable conditions for HCA deposition.

This release of calcium ions and soluble silica is linked to activation of several families of genes in human bone cells and promotion of hydroxyapatite deposition and stimulation of vascularised bone growth on these bioactive glass surfaces. A release of calcium ions triggering or signalling cell-genetic events is well documented.⁴⁹ The solubility and degradation behaviours associated with NBOs are crucial in determining the bioactivity of the materials. A given level of NBOs is linked to a specific rate of release of bioactive ions and therefore is central to the optimal bioactive properties of these glasses. The silicate networks are also connected through BOs which are largely responsible for maintaining the mechanical properties of the materials under both *in vitro* and *in vivo* conditions. Hence it is important to achieve the right balance of BO and NBO to produce optimal bioactivity and mechanical properties in these materials. This also helps to explain the reasons that some particular compositions of silicate-based bioactive glasses (for example 70S30C) produce much better bioactivities than other compositions.

^{31}P is a very sensitive nucleus with 100% natural abundance and a relatively large magnetic moment. This makes ^{31}P NMR an excellent probe nucleus for understanding bioactivity of the materials by the formation of HCA after reaction with SBF solution, despite this layer forming only a small fraction of the sample. The samples studied for apatite formation in SBF reaction include the three different compositions examined above, as well as three additional samples: (i) 100S, a pure silica sol-gel sample without any calcium metal, (ii) 70S30C(a) as above, but heat treated to 1000 °C (therefore containing many fewer surface $-\text{OH}$ groups) and (iii) wollastonite, the crystalline phase with the identical chemical composition to 50S50C. The NMR data are summarised in Table 3. Typical ^{31}P MAS NMR spectra after reaction with SBF are shown in Fig. 11. The ^{31}P resonance in all samples appears at around 2.8-3.6 ppm and can be attributed to hydroxyapatite/HCA. This is verified by comparison with the literature and data determined here for the ^{31}P chemical shift from crystalline hydroxyapatite which displays a narrow resonance at the same position.^{14,50} The

results show that the rate of SBF reaction with these bioactive glasses is fast as HCA formation determined through the presence of the ^{31}P peak can be observed after reaction of only 0.5 hours (Fig. 11a).

It seems that the basic requirement of hydroxyapatite formation for these materials is the existence of surface Si-OH groups, which provide the anchor points for heterogeneous nucleation and crystal growth and the presence of calcium and phosphate ions in solution. This is indicated by a pure silica sample 100S which also shows hydroxyapatite formation after reaction with SBF for 1 hour. The results indicate that rates of the reaction are influenced by concentrations of protons (and thereby assumed largely to be surface Si-OH) in the materials. The materials with a much lower concentration of protons show the reaction being slowed down, especially in the early reaction stages. Two samples, β -wollastonite and 70S30C(a), both with low proton concentrations, show almost no ^{31}P NMR signal after 1 hour reaction, although all samples eventually show hydroxyapatite formation after reaction with SBF for 24 hours. This suggests possibly a longer induction period related to nucleation and/or surface re-hydration in the lower proton-content samples. However, samples with higher NBO contents (i.e. CaO molar ratio 0.2-0.5) show stronger bioactivity and reaction. The rapid release of Ca^{2+} ions promotes surface hydration, and under *in vitro* condition means that a higher degree of supersaturation with respect to hydroxyapatite around the material surface/interface can help to bring about nucleation and deposit an apatite layer. Under *in vivo* conditions, release of calcium ions and soluble silica in specific concentrations also triggers a range of cell level interactions leading to activation of several families of genes in human cells and subsequent bone growth.

The surface structure of these materials can show subtle influences towards the apatite formed. This is demonstrated by the apatite formed on crystalline wollastonite (Fig. 11d) where ^{31}P MAS NMR shows the presence of three relatively narrow resonances, which implies the presence of three different sites. The main resonance is resolved into two lines at 3.6 and 0.7 ppm respectively with nearly equal intensity, while a small peak at -8.2 ppm is seen that was not detected in the other samples. This -8.2 ppm peak probably indicates the formation of a small amount of pyrophosphate. The FWHM of the central resonances after deconvolution is about 330 Hz, which is very close to 300 Hz found in crystalline hydroxyapatite/HCA. This indicates that the apatite formed on wollastonite is in a more ordered/crystalline form. The FWHM of the ^{31}P resonance from the other samples ranges from 800-1000 Hz, with most of them ~ 900 Hz. This is ~ 3 times that of highly crystalline HCA, but is considerably narrower than amorphous phosphates with linewidths of >1500 Hz. Computer modelling indicates that the degree of structural order is strongly driven by

the ordering of the hydroxyls.^{51,52} In studies of some low phosphorus content (4 mol%) calcium phosphate glasses showed that the ratio between calcium and phosphorus seems to be a key factor. This ratio determines both the texture of the bioactive glasses and the chemical nature of the species present at the surface and hence the consequent reactivity of the surfaces.⁵³ That study reacted the powders with water whereas here we used SBF which contains phosphate species. There is a commonly accepted belief that the form of apatite deposited on the surface of these bioactive glasses is an amorphous phase initially, and then grows into a more crystalline one later. Although this possibility cannot be ruled out here, the data from ³¹P solid state NMR indicates that the initial HCA forming is quite ordered and not completely disordered. This suggests that a partially crystalline HCA phase is laid down in the early stages of reaction with SBF, although diffraction tends to suggest it is disordered/amorphous at this stage. It is possible that the apparent difference arises because of the varying length scale sensitivity of the different techniques. Diffraction (especially X-ray and neutron) is sensitive to longer lengths scales than NMR. Phases can appear effectively "amorphous" to diffraction, but are often in the form of very small nanocrystals which show up as quite sharp, although not fully crystalline peaks in NMR. This has been observed for a detailed study of sol-gel formed nanocrystalline ZrO₂ that compared ¹⁷O MAS NMR with diffraction.⁵⁴

4. Conclusions

The structural evolution of sol-gel prepared bioactive calcium silicate materials during heat treatment and in subsequent reaction with simulated body fluid has been effectively probed by a multinuclear solid-state NMR method. The ¹⁷O NMR results reveal the gradual development of NBO with increasing temperature beginning at around 350 °C. At higher temperatures (≥ 500 °C), NBO formation by calcium cations begins to dominate the structural changes, gradually breaking down the silicate network. The intensity of NBO resonance increases with increasing Ca/Si ratio in the materials as well as with temperature. This is confirmed by ²⁹Si NMR data showing increasing Q² and Q³ resonances associated with increasing CaO content after heating at 500 °C. ¹⁷O solid state NMR proved to be a very sensitive probe of bridging and non-bridging oxygen, with the MAS NMR spectra giving complete resolution of these species in this system.

Multinuclear solid state NMR also showed that the bioreactivity with respect to SBF reaction of sol-gel prepared calcium silicates depend strongly on the proton content and that the presence of calcium aids HCA formation via promotion of surface hydration. The dissolution mechanism revealed by ¹⁷O NMR shows the rapid loss of NBO as calcium is

leached from the silicate resulting in changes in connectivity of silicate framework, and indicates the importance of achieving the right balance of BO and NBO for optimal biochemical and mechanical properties. ^{31}P NMR confirmed formation of an HCA layer and suggests that it has quite a high degree of crystallinity. The nature of the silicate surface influences the nature of the phosphate phases formed. These results emphasise that an atomic scale probe such as solid state NMR is essential for detailed understanding of the structural development, bioactivity and dissolution mechanism in such materials.

Acknowledgements

The authors thank the EPSRC for funding on bioactive silicate materials grants GR/R59298 and GR/R57492. MES and JVH thank the University of Warwick, EPSRC and the Birmingham Science City for contribution to the solid state MAS NMR instrumentation used in this research. This was partially supported through the Birmingham Science City Advanced Materials Project 1: Creating and Characterising Next generation Materials Project, with support from Advantage West Midlands (AWM) and partial funding from the European Regional Development Fund (ERDF). Dr Andy Howes is thanked for locating some of the original proton data for reprocessing.

References

1. L. L. Hench, *J. Am Ceram. Soc.*, 1991, **74**, 1487.
2. L. L. Hench, *Biomaterials*, 1998, **19**, 1419.
3. Y. Ebisawa, T. Kokubo, K. Ohura and T. Yamamuro. *J. Mater. Sci. Mater. Med.*, 1990, **1**, 239.
4. I. Izquierdo-Barba, A. J. Salinas and M. Vallet-Regi, *J. Biomed. Mater. Res.*, 1999, **47**, 243.
5. P. Sepulveda, J. R. Jones and L. L. Hench, *J. Biomed. Mater. Res.*, 2002, **59**, 340.
6. S. Lin, C. Ionescu, K. J. Pike, M. E. Smith and J. R. Jones, *J. Mater. Chem.*, 2009, **19**, 1276.
7. R. A. Martin, S. Yue, J. V. Hanna, P. D. Lee, R. J. Newport, M. E. Smith and J. R. Jones, *Phil. Trans. Roy. Soc. A*, 2012, **370**, 1422.
8. J. R. Jones, *Acta Biomater.*, 2013, **9**, 4457.
9. J. R. Jones, L. M. Ehrenfried and L. L. Hench, *Biomaterials*, 2006, **27**, 964.
10. J. R. Jones, O. Tsigkou, E. E. Coates, M. M. Stevens, J. M. Polak and L. L. Hench, *Biomaterials*, 2007, **28**, 1653.
11. J. E. Gough, J. R. Jones and L. L. Hench, *Biomaterials*, 2004, **25**, 2039.
12. T. Tekezawa, *Biomaterials*, 2003, **24**, 2267.
13. L. J. Skipper, F. E. Sowrey, D. M. Pickup, V. Fitzgerald, R. Rashid, K. O. Drake, Z. Lin, P. Saravanapavan, L. L. Hench, M. E. Smith and R. J. Newport, *J. Biomed. Mat. Res.*, 2004, **70A**, 354.

14. L. J. Skipper, F. E. Sowrey, R. Rashid, R. J. Newport, Z. Lin and M. E. Smith, *Phys. Chem. Glasses*, 2005, **46**, 372.
15. R. J. Newport, L. J. Skipper, D. Carta, D. M. Pickup, F. E. Sowrey, M. E. Smith, P. Saravanapavan and L. L. Hench, *J. Mater. Sci.: Mater. Med.*, 2006, **17**, 1003.
16. B. Yu, C. A. Turdean-Ionescu, R. A. Martin, R. J. Newport, J. V. Hanna, M. E. Smith and J. R. Jones, *Langmuir*, 2012, **28**, 17465.
17. I. D. Xynos, A. J. Edgar, L. D. K. Buttery, L. L. Hench and J. M. Polak, *J. Biomed. Mater. Res.*, 2001, **55**, 151.
18. O. Tsigkou, J. R. Jones, J. M. Polak and M. M. Stevens, *Biomaterials*, 2009, **30**, 3542.
19. L. L. Hench, R. J. Splinter, W. C. Allen and T. K. Greenlee, *J. Biomed. Mater. Res. Symp.*, 1971, **5**, 117.
20. S. Midha, T. B. Kim, W. van den Bergh, P. D. Lee J. R. Jones and C. A. Mitchell, *Acta Biomater.*, 2013, **9**, 9169.
21. K. J. D. MacKenzie and M. E. Smith, *Multinuclear Solid State NMR of Inorganic Materials*, Pergamon Press, Oxford, 2002.
22. J. V. Hanna and M. E. Smith, *Solid State Nucl. Magn. Reson.*, 2010, **38**, 1.
23. S. E. Ashbrook and M. E. Smith, *Chem. Soc. Rev.*, 2006, **35**, 718.
24. H. K. C. Timken, S. E. Schramm, R. J. Kirkpatrick and E. Oldfield, *J. Phys. Chem.*, 1987, **91**, 1054.
25. X. D. Cong and R. J. Kirkpatrick, *J. Am. Ceram. Soc.*, 1996, **79**, 1585.
26. P. J. Dirken, S. C. Kohn, M. E. Smith and E. R. H. van Eck, *Chem. Phys. Lett.*, 1997, **266**, 568.
27. J. R. Allward, S. K. Lee and J. F. Stebbins, *Amer. Mineralog.*, 2003, **88**, 949.
28. J. M. Griffin, and S. E. Ashbrook, *Ann. Rep. NMR Spectrosc.*, 2013, **79**, 241.
29. T. J. Bastow, P. J. Dirken, M. E. Smith and H. J. Whitfield, *J. Phys. Chem.*, 1996, **100**, 8539.
30. N. Kim and J. F. Stebbins, *Chem. Mater.*, 2009, **21**, 309.
31. D. S. Middlemiss, F. Blanc, C. J. Pickard and C. P. Grey, *J. Magn. Reson.*, 2010, **204**, 1.
32. P. J. Dirken, M. E. Smith and H. J. Whitfield, *J. Phys. Chem.*, 1995, **99**, 395.
33. D. M. Pickup, G. Mountjoy, G. W. Wallidge, R. J. Newport and M. E. Smith, *Phys. Chem. Chem. Phys.*, 1999, **1**, 2527.
34. D. M. Pickup, G. Mountjoy, M. A. Holland, G. W. Wallidge, R. J. Newport and M. E. Smith, *J. Mater. Chem.*, 2000, **10**, 1887.
35. P. N. Gunawidjaja, M. A. Holland, G. Mountjoy, D. M. Pickup, R. J. Newport and M. E. Smith, *Solid State Nucl. Magn. Reson.*, 2003, **23**, 88.
36. T. Kokubo and H. Takadama, *Biomaterials*, 2006, **27**, 2907.
37. M. Bohner and J. Lemaitre, *Biomaterials*, 2009, **30**, 2175.
38. A. C. Kunwar, G. L. Turner and E. Oldfield, *J. Magn. Reson.*, 1986, **69**, 124.
39. J. P. Amoureux, C. Fernandez and S. Steuernagel, *J. Magn. Reson. A*, 1996, **123**, 116.
40. S. P. Brown and S. Wimperis, *J. Magn. Reson.*, 1997, **128**, 42.
41. J. P. Amoureux and C. Fernandez, *Solid State Nucl. Magn. Reson.*, 1998, **10**, 211.
42. M. E. Smith, and E. R. H. van Eck, *Prog. Nucl. Magn. Reson. Spectrosc.*, 1999, **34**, 159.
43. Y. Millot and P. P. Man, *Solid State Nucl. Magn. Reson.*, 2002, **21**, 21.
44. E. R. H. van Eck, M. E. Smith and S. C. Kohn, *Solid State Nucl. Magn. Reson.*, 1999, **15**, 181.
45. G. Engelhardt and D. Michel, *High resolution solid state NMR of silicates and zeolites*, Wiley, Chichester, 1987.
46. Z. Lin, M. E. Smith, F. E. Sowrey and R. J. Newport, *Phys. Rev. B*, 2004, **69**, 224107.
47. D. Laurencin and M. E. Smith, *Prog. Nucl. Magn. Reson. Spectrosc.*, 2013, **68**, 1.
48. I. L. Moudrakovski, *Ann. Rep. NMR Spectrosc.*, 2013, **79**, 129.
49. L. L. Hench and J. M. Polak, *Science*, 2002, **295**, 1014..

50. D. Laurencin, N. Almora-Barrios, N. H. de Leeuw, C. Gervais, C. Bonhomme, F. Mauri, W. Chrzanowski, J. C. Knowles, R. J. Newport, A. Wong, Z. Gan and M. E. Smith, *Biomaterials*, 2011, **32**, 1826.
51. N. de Leeuw, *Chem. Comm.*, 2001, 1646.
52. N. de Leeuw, *Phys. Chem. Chem Phys.*, 2002, **4**, 3865.
53. M. Cerruti, G. Magnacca, V. Bolis and C. Morterra, *J. Mater. Chem.*, 2003, **13**, 1279.
54. A. V. Chadwick, G. Mountjoy, V. M. Nield, I. J. F. Poplett, M. E. Smith, J. H. Strange and M. G. Tucker, *Chem. Mater.*, 2001, **13**, 1219.

Tables

Table 1 BO and NBO content, δ_{iso} , χ_{Q} and η data of ^{17}O MAS NMR for CaO-SiO₂ materials after heat treatment at 500 °C

Samples	Heat treatment/ °C	BO				NBO			
		<i>I</i> %	δ_{iso} (ppm)	χ_{Q} (MHz)	η	<i>I</i> %	δ_{iso} (ppm)	χ_{Q} (MHz)	η
80S20C	500	93	38	4.9	0.2	7.0	106	3.0	0.4
70S30C	500	79	53	4.25	0.8	21	115	3.1	0.5
50S50C	500	50	64	4.15	0.8	50	131	3.3	0.5

* *I* and δ_{iso} represent relative intensity and isotropic chemical shift respectively. Errors: *I* \pm 5%, δ_{iso} \pm 5 ppm, χ_{Q} \pm 0.1 MHz, η \pm 0.2. For the NMR interaction parameters estimated here these are the mean values of what is a distribution of values given the disordered nature of the sample. The mean values are sufficient to determine the nature of the associated oxygen and no attempt to determine the distribution is made here.

Table 2 Qⁿ content and chemical shift data from ^{29}Si MAS NMR for CaO-SiO₂ materials

Samples	Heat treatment/ °C	Q ⁴		Q ³		Q ²		NC
		<i>I</i> %	δ (ppm)	<i>I</i> %	δ (ppm)	<i>I</i> %	δ (ppm)	
80S20C	120	68.0	-111.3	29.5	-101.4	2.5	-91.3	3.65
70S30C	120	70.1	-111.0	25.9	-100.6	4.1	-90.0	3.66
50S50C	120	67.7	-110.9	26.9	-101.2	5.4	-91.6	3.62
80S20C	350	68.7	-110.2	28.5	-100.0	2.8	-91.0	3.66
70S30C	350	71.2	-110.0	23.7	-100.0	5.6	-91.0	3.67
50S50C	350	68.1	-110.0	26.0	-100.0	5.9	-90.8	3.62
80S20C	500	69.1	-110.6	27.7	-100.6	3.2	-89.6	3.65
70S30C	500	59.7	-110.5	31.2	-100.0	9.1	-89.0	3.51
50S50C	500	31.3	-110.0	18.3	-96.5	50.4	-78.0	2.81
70S30C	700	47.2	-111.0	24.4	-100.0	28.4	-89.0	3.18

* *I* and δ represent relative intensity and chemical shift respectively.
 NC is the Network Connectivity defined as $(4 \times \%Q^4 + 3 \times \%Q^3 + 2 \times \%Q^2 + \%Q^1)/100$
 Errors: *I* \pm 5%, δ \pm 0.5 ppm and NC \pm 0.05.

Table 3 ^{31}P MAS NMR data after reaction with SBF for 24 hours and quantitative ^1H MAS NMR from calcium silicate samples to determine the proton content.

Samples	Heat treatment/ $^{\circ}\text{C}$	^{31}P δ (ppm)	^{31}P FWHM (Hz)	Proton content per Si
80S20C	500	3.1	950	0.90
70S30C	500	3.4	930	0.77
50S50C	500	3.3	860	0.73
100S	500	2.8	950	0.93
70S30C(a)	1000	3.3	950	0.11
Wollastonite	-	3.3 0.6–8.2	700	0.03

* δ represent chemical shift and FWHM- full width at half maximum. Errors: $\delta \pm 0.2$ ppm, FWHM ± 50 Hz. The proton contents are estimated to have a $\sim 10\%$ error.

Figure Captions

- Figure 1 ^{17}O MAS NMR spectra with heat treatment at 120 °C for (a) 80S20C, (b) 70S30C and (c) 50S50C sample. * indicates higher than expected singularity due to overlap with OH.
- Figure 2 ^{17}O static NMR spectra of 80S20C after heat treatment at (a) 120 and (b) 350 °C. * indicates the OH resonance.
- Figure 3 ^{17}O MAS NMR spectra after heat treatment at 350 °C for (a) 80S20C, (b) 70S30C and (c) 50S50C samples. * indicates higher than expected singularity due to overlap with OH and ↓ indicates the NBO resonance.
- Figure 4 ^{17}O MAS NMR spectra after heat treatment at 500 °C for (a) 80S20C, (b) 70S30C and (c) 50S50C samples.
- Figure 5 ^{17}O MAS NMR spectra of 70S30C after heat treatment at (a) 120, (b) 500 and (c) 700 °C.
- Figure 6 ^{17}O 3Q MAS NMR of 70S30C at 11.7 T after heat treatment at (a) 350 and (b) 600 °C, and at 14.1 T after heat treatment at (a) 350 and (b) 600 °C.
- Figure 7 ^{29}Si MAS NMR spectra of (a) 80S20C, (b) 70S30C and (c) 50S50C after heat treatment at 500 °C.
- Figure 8 ^{29}Si MAS NMR spectra of 70S30C after heat treatment at (a) 120, (b) 500 and (c) 700 °C.
- Figure 9 ^{17}O MAS NMR of 80S20C before and after SBF reaction. (a) before reaction, (b) 1 hour and (c) 24 hours.
- Figure 10 ^1H MAS NMR spectra of samples heated to 500 °C (a) 50S50C, (b) 70S30C, (c) 80S20C and (d) 100S.
- Figure 11 ^{31}P MAS NMR spectra of 70S30C and wollastonite after reaction with SBF. (a) 70S30C/0.5 hr. (b) 70S30C/1 hr. (c) 70S30C/24 hr. (d) wollastonite/24hr.

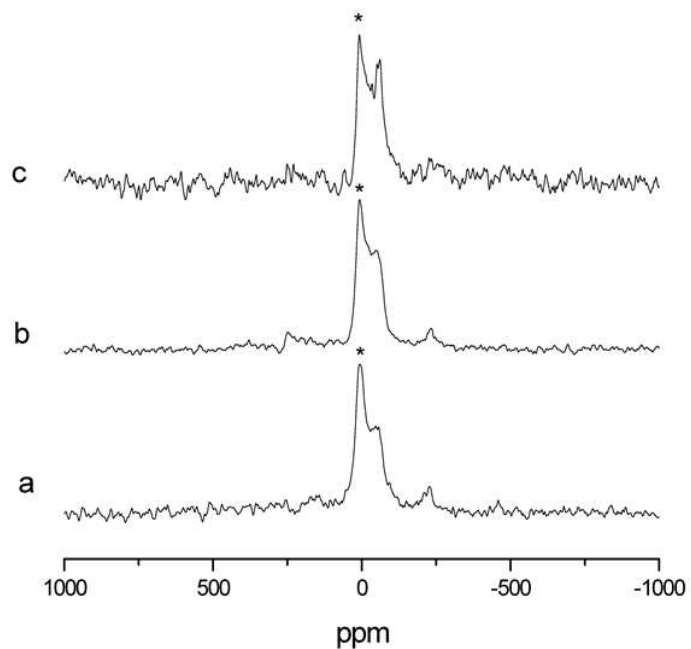


Figure. 1 ^{17}O MAS NMR spectra after heat treatment at 120 °C for (a) 50 80S20C, (b) 70S30C and (c) 50SC samples, * indicates higher than expected singularity due to overlap with OH.

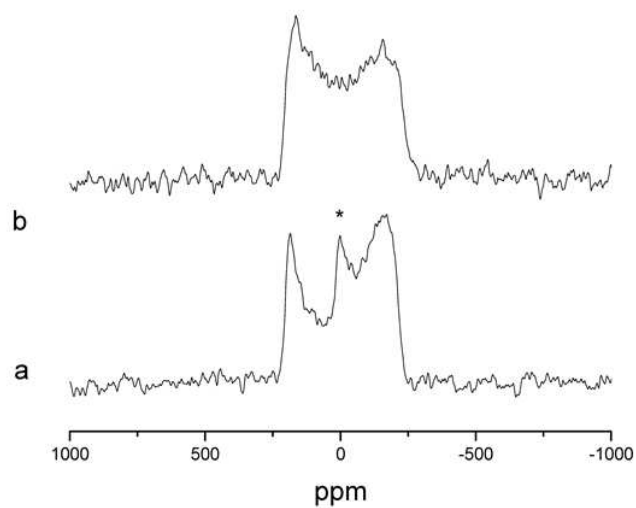


Figure .2 ^{17}O static NMR spectra of 80S20C with heat treatment at (a) 120 and (b) 350 °C. * indicates the OH resonance.

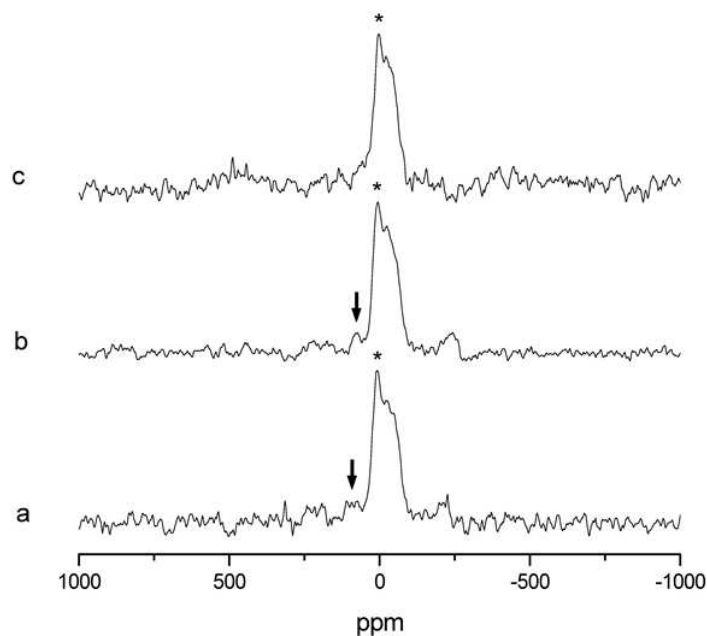


Figure 3 ^{17}O MAS NMR spectra after heat treatment at 350 °C for (a) 80S20C, (b) 70S30C and (c) 50S50C samples. * indicates higher than expected singularity due to overlap with OH and ↓ indicates the NBO resonance.

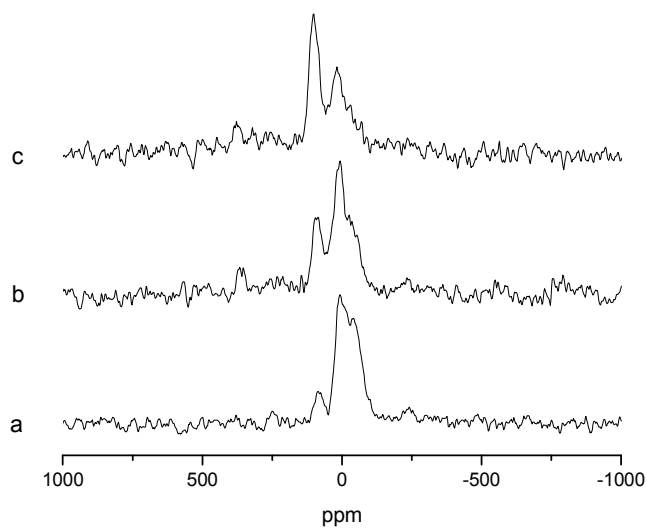


Figure 4 ^{17}O MAS NMR spectra after heat treatment at 500 °C for (a) 80S20C, (b) 70S30C and (c) 50S50C samples.

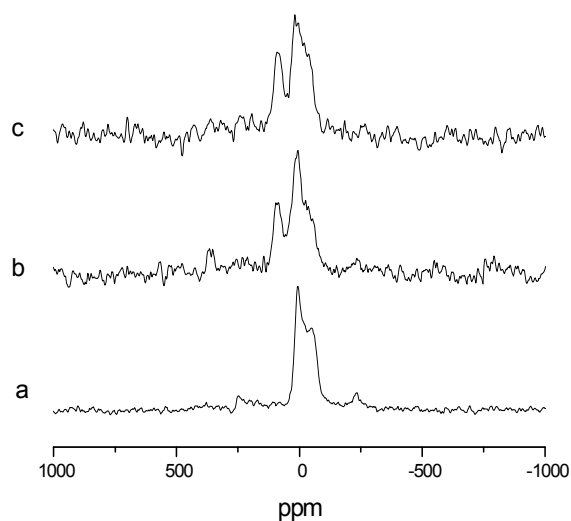


Figure 5 ^{17}O MAS NMR spectra of 70S30C after heat treatment at (a) 120, (b) 500 and (c) 700 $^{\circ}\text{C}$.

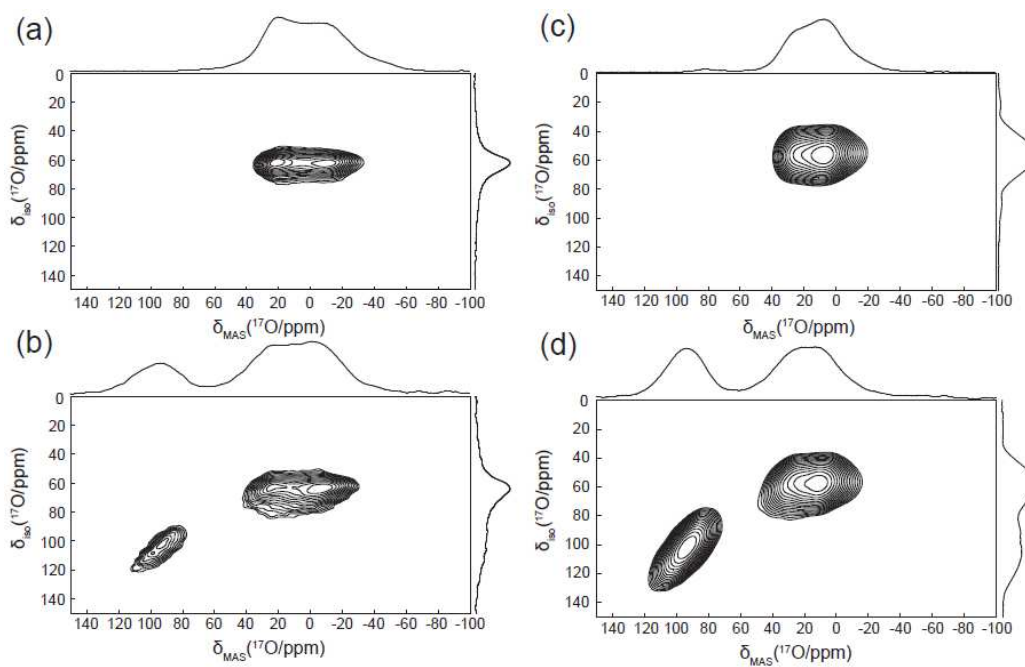


Figure 6 ^{17}O 3Q MAS NMR of 70S30C at 11.7 T after heat treatment at (a) 350 and (b) 600 $^{\circ}\text{C}$, and at 14.1 T after heat treatment at (c) 350 and (d) 600 $^{\circ}\text{C}$.

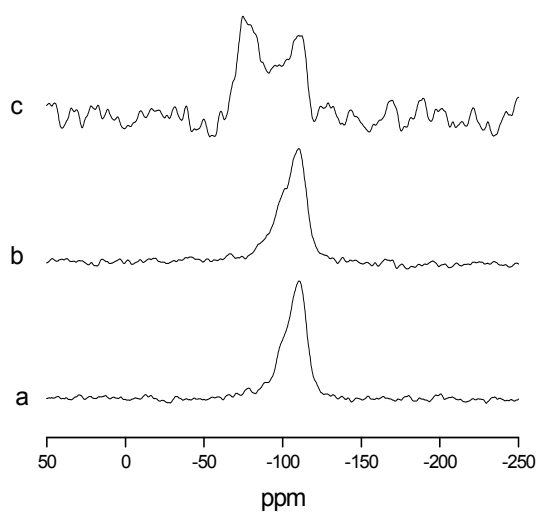


Figure 7 ^{29}Si MAS NMR spectra of (a) 80S20C, (b) 70S30C and (c) 50S50C samples after heat treatment at 500 °C.

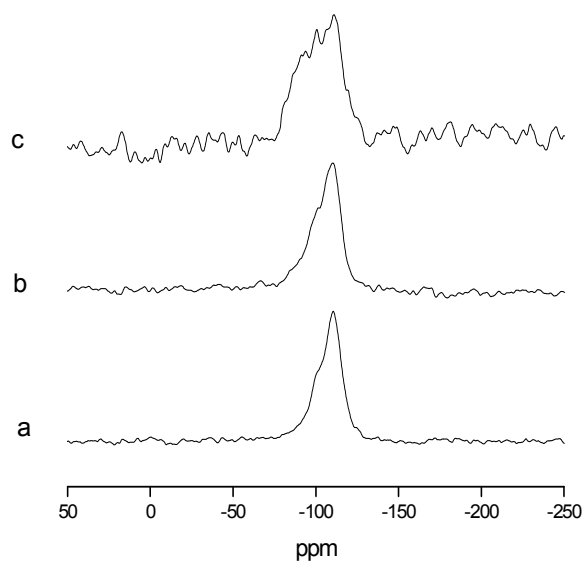


Figure 8 ^{29}Si MAS NMR spectra of 70S30C after heat treatment at (a) 120, (b) 500 and (c) 700 °C.

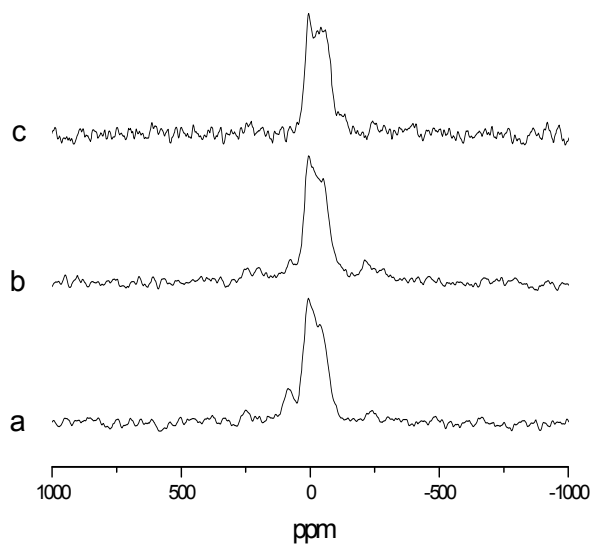


Figure 9 ^{17}O MAS NMR of 80S20C before and after SBF reaction. (a) before reaction, (b) 1 hour and (c) 24 hours.

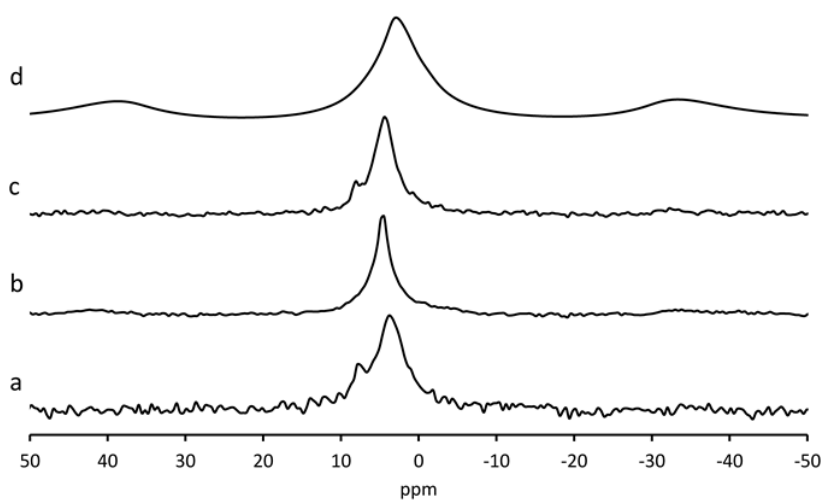


Figure 10 ^1H MAS NMR spectra of samples heated to 500 °C (a) 50S50C, (b) 70S30C, (c) 80S20C and (d) 100S.

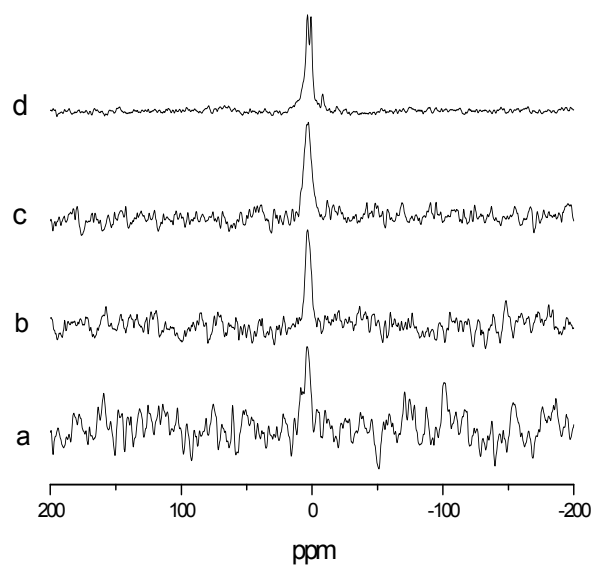


Figure 10 ^{31}P MAS NMR spectra of 70S30C and wollastonite after reaction with SBF. (a) 70S30C /0.5 hr, (b) 70S30C /1 hr, (c) 70S30C /24 hr and (d) wollastonite/24hr.

Table of Contents

Multinuclear solid state NMR, especially ^{17}O , shows the structural evolution of calcium silicate sol-gel bioactive glasses during stabilisation and subsequent reaction with simulated body fluid.

